

Higgs-Boson Production Associated with a Single Bottom Quark in Supersymmetric QCD

Hou Hong-Sheng², Ma Wen-Gan^{1,2}, Wu Peng², Wang Lei² and Zhang Ren-You²

¹CAST (World Laboratory), P.O.Box 8730, Beijing, 100080, People's Republic of China

²Department of Modern Physics, University of Science and Technology of China (USTC),
Hefei, Anhui 230027, People's Republic of China

Abstract

Due to the enhancement of the couplings between Higgs boson and bottom quarks in the minimal supersymmetric standard model (MSSM), the cross section of the process $pp(p\bar{p}) \rightarrow h^0 b(h^0 \bar{b}) + X$ at hadron colliders can be considerably enhanced. We investigated the production of Higgs boson associated with a single high- p_T bottom quark via subprocess $bg(\bar{b}g) \rightarrow h^0 b(h^0 \bar{b})$ at hadron colliders including the next-to-leading order (NLO) QCD corrections in MSSM. We find that the NLO QCD correction in the MSSM reaches 50% \sim 70% at the LHC and 60% \sim 85% at the Fermilab Tevatron in our chosen parameter space.

PACS: 14.80.Ly, 11.30.Pb, 12.60.Jv

I. INTRODUCTION

One of the most important tasks of future high-energy experiments is to search for scalar Higgs particles and investigate the symmetry breaking mechanism of the electroweak $SU(2) \times U(1)$. In the standard model (SM) [1], one doublet of complex scalar fields is needed to spontaneously break the symmetry, leading to a single neutral Higgs boson h^0 . But there exists the problem of the quadratically divergent contributions to the corrections to the Higgs boson mass. This is the so-called naturalness problem of the SM. One of the good methods to solve this problem is to make supersymmetric (SUSY) extensions to the SM. Then the quadratic divergences of the Higgs mass can be cancelled by loop diagrams involving the supersymmetric partners of the SM particles exactly. The most attractive supersymmetric extension of the SM is the minimal supersymmetric standard model (MSSM) [2, 3]. In the MSSM, there are two Higgs doublets H_1 and H_2 to give masses to up- and down-type fermions. The Higgs sector consists of three neutral Higgs bosons, one CP -odd particle (A^0), two CP -even particles (h^0 and H^0), and a pair of charged Higgs bosons (H^\pm).

In the SM, the so-called Yukawa couplings describe the interactions between Higgs and fermions. Their coupling strengths are proportional to m_f/v , where v is the vacuum expectation value of the Higgs field. Since the bottom quark mass is approximately 5 GeV, the Yukawa coupling to bottom quarks is relatively weak. This leads to a small cross section for the associated production of the Higgs boson (h^0) and bottom quarks at hadron colliders [4, 5]. However, in the MSSM, the Yukawa coupling between the Higgs boson (h^0) and bottom quarks can be considerably enhanced for large values of $\tan\beta = v_2/v_1$, where v_1 and v_2 are the vacuum expectation values of the two Higgs boson fields H_1 and H_2 , respectively.

Because the high- p_T bottom quark can be tagged with reasonably high efficiency, the observation of a bottom quark with high p_T can reduce the backgrounds of the Higgs boson production. The leading-order subprocess for production of the Higgs boson associated with bottom quark is $bg \rightarrow bh^0$ [6]. Recently, the investigations of the process $pp(p\bar{p}) \rightarrow bg(\bar{b}g) \rightarrow h^0b(h^0\bar{b}) + X$ in the SM including

the NLO QCD corrections is presented in Ref. [7]. Their calculation shows the cross section of the subprocess of $bg \rightarrow h^0b$ is an order of magnitude larger than those of $gg(q\bar{q}) \rightarrow b\bar{b}h^0$ at the Fermilab Tevatron and the CERN LHC. They find that the NLO QCD correction ranges from 50-60% at the Tevatron for $m_h = 100 - 200$ GeV, and at the LHC the correction with $m_h = 120 - 500$ GeV ranges from 20 - 40% for $p_T > 15$ GeV and 25 - 45% for $p_T > 30$ GeV. They conclude that this production mechanism improves the prospects for the discovery of a Higgs boson with enhanced coupling to the bottom quarks.

In this paper, we calculated the cross section for the associated production of the Higgs boson and a single high- p_T bottom quark via $bg \rightarrow h^0b(\bar{b}g \rightarrow h^0\bar{b})$ in the MSSM at the Tevatron and the LHC including the NLO QCD corrections. The structure of this paper is as follow: In Sec. II, we discuss the LO results of the subprocess $bg \rightarrow h^0b$. In Sec. III, we present the calculations of the NLO QCD corrections. In Sec. IV, the numerical results and conclusions are presented. Some lengthy analytical expressions are listed in Appendices.

II. THE LEADING ORDER CROSS SECTION

Since the cross sections for the subprocess $bg \rightarrow h^0b$ and its charge-conjugate subprocess $\bar{b}g \rightarrow h^0\bar{b}$ in the CP-conserved MSSM are same, we present only the calculation of the subprocess $b(p_1)g(p_2) \rightarrow h^0(k_3)b(k_4)$ here (where $p_{1,2}$ and $k_{3,4}$ represent the four-momentum of the incoming partons and the outgoing particles, respectively.). The subprocess $bg \rightarrow h^0b$ can occur through both s-channel and t-channel as shown in Fig.1(A-B). So we divide the tree-level amplitude into two parts and denote it as

$$M^0 = M_0^{(s)} + M_0^{(t)}, \quad (2.1)$$

where $M_0^{(s)}$ and $M_0^{(t)}$ represent the amplitudes arising from the s-channel diagram shown in Fig.1(A) and the t-channel diagram shown in Fig.1(B) at the tree-level, respectively. The explicit expressions

for the amplitudes $M_0^{(s)}$ and $M_0^{(t)}$ can be written as

$$\begin{aligned} M_0^{(s)} &= \frac{g_s(\mu_r)Y_b(\mu_r)}{\hat{s}}\bar{u}_i(k_4)(\not{p}_1 + \not{p}_2)\gamma_\nu u_j(p_1)\epsilon_\nu(p_2)T_{ij}^a, \\ M_0^{(t)} &= \frac{g_s(\mu_r)Y_b(\mu_r)}{\hat{t}}\bar{u}_i(k_4)\gamma_\nu(\not{p}_1 - \not{k}_3)u_j(p_1)\epsilon_\nu(p_2)T_{ij}^a, \end{aligned} \quad (2.2)$$

where $\hat{s} = (p_1 + p_2)^2$, $\hat{t} = (p_1 - k_3)^2$ and $\hat{u} = (p_1 - k_4)^2$ are the usual Mandelstam variables. $g_s(\mu_r)$ is the running strong coupling strength and T^a is the $SU(3)$ color matrix. $Y_b(\mu_r)$ is the Yukawa coupling between Higgs boson and bottom quarks. In MSSM, $Y_b(\mu_r)$ is given as

$$Y_b(\mu_r) = i\frac{g_w\overline{m}_b(\mu_r)}{2m_W}\frac{\sin\alpha}{\cos\beta}, \quad (2.3)$$

where α is the mixing angle which leads to the physical Higgs eigenstates h^0 and H^0 . $\overline{m}_b(\mu_r)$ is the $\overline{\text{MS}}$ mass of the bottom quark. Throughout our evaluation we adopt the simplified Aivazis-Collins-Olness-Tung(ACOT) scheme[8], which will not make loss of accuracy in our calculation of subprocess $bg \rightarrow h^0b$. That means the bottom quark mass is neglected except in the Yukawa couplings during our calculation.

Then the lowest order cross section for the subprocess $bg \rightarrow h^0b$ in the MSSM is obtained by using the following formula:

$$\hat{\sigma}^0(\hat{s}, bg \rightarrow h^0b) = \frac{1}{16\pi\hat{s}^2} \int_{\hat{t}_{min}}^{\hat{t}_{max}} d\hat{t} \overline{\sum} |M^0|^2, \quad (2.4)$$

where $\hat{t}_{max} = 0$ and $\hat{t}_{min} = m_h^2 - \hat{s}$. The summation is taken over the spins and colors of initial and final states, and the bar over the summation recalls averaging over the spins and colors of initial partons.

III. NLO QCD CORRECTIONS

The NLO QCD contributions to the associated production of the Higgs boson and a single bottom quark can be separated into two parts: the virtual corrections arising from loop diagrams and the real gluon emission corrections.

1. Virtual Corrections

The virtual corrections in the MSSM to $bg \rightarrow h^0 b$ consist of self-energy, vertex and box diagrams which are shown in Figs.2-3. Fig.2 shows the one-loop diagrams of the SM-like QCD corrections from quarks and gluons, and Fig.3 presents the one-loop diagrams of the SUSY QCD corrections from squarks and gluinos. There exist both ultraviolet(UV) and soft/collinear infrared(IR) singularities in the amplitude from the SM-like diagrams in Fig.2, and the amplitude part from SUSY QCD diagrams(Fig.3) only contains UV singularities. In our calculation, we adopt the 't Hooft-Feynman gauge and all the divergences are regularized by using dimensional regularization method in $d = 4 - 2\epsilon$ dimensions.

In order to remove the UV divergences, we need to renormalize the wave functions of the external fields, the strong coupling and the $h^0 - b - \bar{b}$ Yukawa coupling. For the renormalization of the strong and Yukawa couplings, we employ the modified Minimal Subtraction ($\overline{\text{MS}}$) scheme. The relevant renormalization constants in this work are defined as

$$\begin{aligned}
 m_b &\rightarrow m_b + \delta m_b, \quad g_s \rightarrow (1 + \delta g_s) g_s \\
 Y_b &\rightarrow Y_b + \delta Y_b, \quad \delta Y_b = Y_b \frac{\delta m_b}{m_b} \\
 b &\rightarrow \left(1 + \frac{1}{2} \delta Z_b\right) b \\
 g_\mu &\rightarrow (1 + \frac{1}{2} \delta Z_g) g_\mu,
 \end{aligned} \tag{3.1}$$

where g_s and Y_b denote the strong coupling and the $h - b - \bar{b}$ Yukawa coupling. b and g_μ denote the fields of bottom quark and gluon. The explicit expressions of these renormalization constants are presented in Appendix A.

Then the renormalized amplitude for virtual corrections, M^V , can be divided into two parts and expressed as

$$M^V = M^{\text{loop}} + M^{\text{CT}}, \tag{3.2}$$

where M^{loop} is the amplitude from one loop-diagrams shown in Figs.2-3 and M^{CT} is the amplitude from the diagrams which contain counter-terms shown in Fig.4. The expression of the M^{loop} can be written in the form as

$$\begin{aligned} M^{loop} = & \bar{u}_i(k_4)[f_1\gamma_\mu P_L + f_2\gamma_\mu P_R + f_3p_{1\mu}P_L + f_4p_{1\mu}P_R + f_5k_{4\mu}P_L + f_6k_{4\mu}P_R + f_7p_{1\mu}p_2P_L \\ & + f_8p_{1\mu}p_2P_R + f_9k_{4\mu}p_2P_L + f_{10}k_{4\mu}p_2P_R + f_{11}\gamma_\mu p_2P_L + f_{12}\gamma_\mu p_2P_R]u_j(p_1)\epsilon_\mu(p_2)T_{ij}^a, \end{aligned} \quad (3.3)$$

where $P_{L,R} = \frac{1 \mp \gamma_5}{2}$. The explicit expressions of form factors f_i ($i = 1 \sim 12$) are presented in Appendix B, and M^{CT} is expressed in Appendix A.

The virtual corrections to the cross section can be written as

$$\hat{\sigma}^V(\hat{s}, bg \rightarrow h^0 b) = \frac{1}{16\pi\hat{s}^2} \int_{\hat{t}_{min}}^{\hat{t}_{max}} d\hat{t} 2Re \overline{\sum} [(M^V)^\dagger M^0], \quad (3.4)$$

with $\hat{t}_{max} = 0$ and $\hat{t}_{min} = m_h^2 - \hat{s}$ and again the summation with bar means the same operations as appeared in Eq.(2.4).

After the renormalization procedure, $\hat{\sigma}^V$ is UV-finite. Nevertheless, it still contains the soft/collinear IR singularities

$$d\hat{\sigma}^V|_{IR} = \left[\frac{\alpha_s}{2\pi} \frac{\Gamma(1-\epsilon)}{\Gamma(1-2\epsilon)} \left(\frac{4\pi\mu_r^2}{\hat{s}} \right)^\epsilon \right] d\hat{\sigma}^0 \left(\frac{A_2^V}{\epsilon^2} + \frac{A_1^V}{\epsilon} \right), \quad (3.5)$$

where

$$\begin{aligned} A_2^V &= -\frac{17}{3}, \\ A_1^V &= -\frac{47}{6} + 3\ln\frac{-\hat{t}}{\hat{s}-m_h^2} - \frac{1}{3}\ln\frac{-\hat{u}}{\hat{s}-m_h^2}. \end{aligned} \quad (3.6)$$

The soft divergences can be cancelled by adding with the soft real gluon emission corrections, and the remaining collinear divergences are absorbed into the parton distribution functions, which will be discussed in the following subsections.

2. Real gluon emission Corrections

The $O(\alpha_s)$ corrections to $bg \rightarrow h^0b$ due to real gluon emission (shown in Fig.5) give the origin of IR singularities which cancel exactly the analogous singularities present in the $O(\alpha_s)$ virtual corrections mentioned in above subsection. These singularities can be either of soft or collinear nature and can be conveniently isolated by slicing the $bg \rightarrow h^0b + g$ phase space into different regions defined by suitable cutoffs, a method which goes under the general name of Phase Space Slicing(PPS). In this paper, we have calculated the cross section for the $2 \rightarrow 3$ process

$$b(p_1) + g(p_2) \rightarrow h^0(k_3) + b(k_4) + g(k_5), \quad (3.7)$$

using the method named two cutoff phase space slicing method[9]. We define the invariants

$$\begin{aligned} \hat{s} &= (p_1 + p_2)^2, \quad \hat{t} = (p_1 - k_3)^2, \quad \hat{u} = (p_1 - k_4)^2, \\ \hat{s}_{45} &= (k_4 + k_5)^2, \quad \hat{t}_{15} = (p_1 - k_5)^2, \quad \hat{t}_{25} = (p_2 - k_5)^2, \quad \hat{t}_{45} = (k_4 - k_5)^2, \end{aligned} \quad (3.8)$$

and describe this method briefly as follows. Firstly, by introducing an arbitrary small soft cutoff δ_s we separate the $2 \rightarrow 3$ phase space into two regions, according to whether the energy of the emitted gluon is soft, i.e. $E_5 \leq \delta_s \sqrt{\hat{s}}/2$, or hard, i.e. $E_5 > \delta_s \sqrt{\hat{s}}/2$. The partonic real cross section can be written as

$$\hat{\sigma}^R(bg \rightarrow h^0bg) = \hat{\sigma}^S(bg \rightarrow h^0bg) + \hat{\sigma}^H(bg \rightarrow h^0bg), \quad (3.9)$$

where $\hat{\sigma}^S$ is obtained by integrating over the soft region of the emitted gluon phase space, contains all the soft IR singularities. Secondly, to isolate the remaining collinear singularities from $\hat{\sigma}^H$, we further decompose $\hat{\sigma}^H$ into a sum of hard-collinear (HC) and hard-non-collinear ($\overline{\text{HC}}$) terms by introducing another cutoff δ_c named collinear cutoff

$$\hat{\sigma}^H(bg \rightarrow h^0bg) = \hat{\sigma}^{\text{HC}}(bg \rightarrow h^0bg) + \hat{\sigma}^{\overline{\text{HC}}}(bg \rightarrow h^0bg). \quad (3.10)$$

The HC regions of the phase space are those where the invariants t_{15}, t_{25}, t_{45} become smaller in magnitude than $\delta_c \hat{s}$, in collinear condition, while at the same time the emitted gluon remains hard. $\hat{\sigma}^{\text{HC}}$ contains the collinear divergences. In the soft and HC region, $\hat{\sigma}^S$ and $\hat{\sigma}^{\text{HC}}$ can be obtained by

performing the phase space integration in d -dimension analytically. In the $\overline{\text{HC}}$ region, $\hat{\sigma}^{\overline{\text{HC}}}$ is finite and may be evaluated in four dimensions using standard Monte Carlo techniques[10]. The cross sections, $\hat{\sigma}^S$, $\hat{\sigma}^{\text{HC}}$ and $\hat{\sigma}^{\overline{\text{HC}}}$, depend on the two arbitrary parameters, δ_s and δ_c . However, in the total real gluon emission hadronic cross section $\hat{\sigma}^R$, after mass factorization, the dependence on these arbitrary cutoffs cancels, as will be explicitly shown in Sec. IV. This constitutes an important check of our calculation.

In the next two subsections, we will discuss in detail the soft, hard-collinear gluon emission.

2.1 Soft gluon emission

In the $p_1 + p_2$ rest frame, the emitted gluon's d -momentum ($d = 4 - 2\epsilon$) can be parameterized as

$$k_5 = E_5(1, \dots, \sin \theta_1 \sin \theta_2, \sin \theta_1 \cos \theta_2, \cos \theta_1) \quad (3.11)$$

The soft region of the $bg \rightarrow h^0 b + g$ phase space is defined by

$$0 < E_5 \leq \delta_s \sqrt{\hat{s}}/2 \quad (3.12)$$

In the soft region, the three body phase space can be factorized as[9]

$$d\Gamma_3|_{soft} = d\Gamma_2 \left[\left(\frac{4\pi}{\hat{s}} \right)^\epsilon \frac{\Gamma(1-\epsilon)}{\Gamma(1-2\epsilon)} \frac{1}{2(2\pi)^2} \right] dS \quad (3.13)$$

with

$$dS = \frac{1}{\pi} \left(\frac{4}{\hat{s}} \right)^{-\epsilon} \int_0^{\delta_s \sqrt{\hat{s}}/2} dE_5 E_5^{1-2\epsilon} \sin^{1-2\epsilon} \theta_1 d\theta_1 \sin^{-2\epsilon} \theta_2 d\theta_2. \quad (3.14)$$

In the soft limit, the matrix element squared for the real gluon emission, $\overline{\sum} |M^R|^2$, can be factorized into the Born matrix element squared times an eikonal factor Φ_{eik}

$$\overline{\sum} |M^R(bg \rightarrow h^0 b + g)|^2 = (4\pi\alpha_s \mu_r^{2\epsilon}) \overline{\sum} |M^0(bg \rightarrow h^0 b)|^2 \Phi_{eik}, \quad (3.15)$$

where

$$\Phi_{eik} = N \frac{p_1 \cdot p_2}{(p_1 \cdot k_5)(p_2 \cdot k_5)} - \frac{1}{N} \frac{p_1 \cdot k_4}{(p_1 \cdot k_5)(k_4 \cdot k_5)} + N \frac{p_2 \cdot k_4}{(p_2 \cdot k_5)(k_4 \cdot k_5)}, \quad (3.16)$$

with $N = 3$. The partonic differential cross section in the soft region can be written as

$$d\hat{\sigma}^S = (4\pi\alpha_s\mu_r^{2\epsilon}) \left[\left(\frac{4\pi}{\hat{s}} \right)^\epsilon \frac{\Gamma(1-\epsilon)}{\Gamma(1-2\epsilon)} \frac{1}{2(2\pi)^2} \right] d\hat{\sigma}^0 \int dS \Phi_{eik}. \quad (3.17)$$

After integration over the eikonal factors, the differential cross section is

$$d\hat{\sigma}^S = d\hat{\sigma}^0 \left[\frac{\alpha_s}{2\pi} \frac{\Gamma(1-\epsilon)}{\Gamma(1-2\epsilon)} \left(\frac{4\pi\mu_r^2}{\hat{s}} \right)^\epsilon \right] \left(\frac{A_2^S}{\epsilon^2} + \frac{A_1^S}{\epsilon} + A_0^S \right), \quad (3.18)$$

with

$$\begin{aligned} A_2^S &= \frac{17}{3}, \\ A_1^S &= -\frac{34}{3} \ln \delta_s - 3 \ln \frac{-\hat{t}}{\hat{s} - m_h^2} + \frac{1}{3} \ln \frac{-\hat{u}}{\hat{s} - m_h^2}, \\ A_0^S &= \frac{34}{3} \ln^2 \delta_s + 6 \ln \delta_s \ln \frac{-\hat{t}}{\hat{s} - m_h^2} + \frac{3}{2} \ln^2 \frac{-\hat{t}}{\hat{s} - m_h^2} \\ &\quad - \frac{2}{3} \ln \delta_s \ln \frac{-\hat{u}}{\hat{s} - m_h^2} - \frac{1}{6} \ln^2 \frac{-\hat{u}}{\hat{s} - m_h^2} - \frac{1}{3} \text{Li}_2 \left[\frac{-\hat{t}}{\hat{s} - m_h^2} \right] + 3 \text{Li}_2 \left[\frac{-\hat{u}}{\hat{s} - m_h^2} \right]. \end{aligned} \quad (3.19)$$

2.2 Hard collinear gluon emission

In the limit where two of the partons are collinear, the three body phase space is greatly simplified. And in the same limit, the leading pole approximation of the matrix element is valid. According to whether the collinear singularities are initial or final state in origin, we separate $\hat{\sigma}^{\text{HC}}$ into two pieces

$$\hat{\sigma}^{\text{HC}} = \hat{\sigma}_i^{\text{HC}} + \hat{\sigma}_f^{\text{HC}}. \quad (3.20)$$

$\hat{\sigma}_i^{\text{HC}}$ is the cross section arising from the case that the emitted gluon is collinear to the initial partons, $0 \leq t_{15}, t_{25} \leq \delta_c \hat{s}$. And $\hat{\sigma}_f^{\text{HC}}$ arises from the case that the emitted gluon is collinear to the final parton, $0 \leq t_{45} \leq \delta_c \hat{s}$. We will treat $\hat{\sigma}_f^{\text{HC}}$ and $\hat{\sigma}_i^{\text{HC}}$ in Sec. 2.2.1 and Sec. 2.2.2 respectively.

2.2.1 Collinear to the final parton

Let p_4 and p_5 be collinear to each other, $0 \leq t_{45} \leq \delta_c \hat{s}$. In the collinear limit, the three body phase space in $d = 4 - 2\epsilon$ time-space dimensions may be written as[9]

$$d\Gamma_3|_{\text{coll}} = d\Gamma_2 \frac{(4\pi)^\epsilon}{16\pi^2 \Gamma(1-\epsilon)} dz d\hat{s}_{45} [\hat{s}_{45} z (1-z)]^{-\epsilon}. \quad (3.21)$$

The squared matrix element can be factorized as

$$\overline{\sum} |M_f^{\text{HC}}(bg \rightarrow h^0 bg)|^2 \simeq \overline{\sum} |M^0(bg \rightarrow h^0 b)|^2 P_{bb}(z, \epsilon) g_s^2 \mu_r^{2\epsilon} \frac{2}{\hat{s}_{45}}, \quad (3.22)$$

where $P_{bb}(z, \epsilon)$ is the d -dimensional unregulated ($z < 1$) splitting function related to the usual Altarelli-Parisi splitting kernels[11]. $P_{bb}(z, \epsilon)$ can be written explicitly as

$$\begin{aligned} P_{bb}(z, \epsilon) &= P_{bb}(z) + \epsilon P'_{bb}(z), \\ P_{bb}(z) &= C_F \frac{1+z^2}{1-z}, \quad P'_{bb}(z) = -C_F(1-z), \end{aligned} \quad (3.23)$$

with $C_F = 4/3$. After integration over the collinear gluon degrees of freedom, the cross section $\hat{\sigma}_f^{\text{HC}}$ can be written as[9]

$$d\hat{\sigma}_f^{\text{HC}} = d\hat{\sigma}^0 \left[\frac{\alpha_s}{2\pi} \frac{\Gamma(1-\epsilon)}{\Gamma(1-2\epsilon)} \left(\frac{4\pi\mu_r^2}{\hat{s}} \right)^\epsilon \right] \left(\frac{A_1^{b \rightarrow bg}}{\epsilon} + A_0^{b \rightarrow bg} \right), \quad (3.24)$$

where

$$\begin{aligned} A_1^{b \rightarrow bg} &= C_F(3/2 + 2 \ln \delta_s), \\ A_0^{b \rightarrow bg} &= C_F[7/2 - \pi^2/3 - \ln^2 \delta_s - \ln \delta_c(3/2 + 2 \ln \delta_s)]. \end{aligned} \quad (3.25)$$

2.2.2 Collinear to the initial parton

Let the hard gluon be emitted collinear to one of the incoming partons, $0 \leq t_{15} \leq \delta_c \hat{s}_{12}$ or $0 \leq t_{25} \leq \delta_c \hat{s}_{12}$. In this region, the initial state partons $i(i = b, g)$ is considered to split into a hard parton i' and a collinear gluon, $i \rightarrow i'g$, with $p_{i'} = z p_i$ and $k_5 = (1-z)p_i$. The matrix element squared for $bg \rightarrow h^0 bg$ factorizes into the Born matrix element squared and the Altarelli-Parisi splitting function

$$\overline{\sum} |M_i^{\text{HC}}(bg \rightarrow h^0 bg)|^2 \simeq (4\pi\alpha_s\mu_r^{2\epsilon}) \overline{\sum} |M^0(bg \rightarrow h^0 b)|^2 \left(\frac{-2P_{bb}(z, \epsilon)}{z\hat{t}_{15}} + \frac{-2P_{gg}(z, \epsilon)}{z\hat{t}_{25}} \right), \quad (3.26)$$

where

$$\begin{aligned} P_{gg}(z, \epsilon) &= P_{gg}(z) + \epsilon P'_{gg}(z), \\ P_{gg}(z) &= 2N \left[\frac{z}{1-z} + \frac{1-z}{z} + z(1-z) \right], \quad P'_{gg}(z) = 0. \end{aligned} \quad (3.27)$$

Using the approximation $p_i - k_5 \simeq z p_i$ ($i = 1, 2$), the three body phase space may be written as

$$d\Gamma_3|_{coll} = d\Gamma_2 \frac{(4\pi)^\epsilon}{16\pi^2 \Gamma(1-\epsilon)} dz d\hat{t}_{i5} [-(1-z)\hat{t}_{i5}]^{-\epsilon}, \quad (i = 1, 2). \quad (3.28)$$

Note that the two body phase space should be evaluated at a squared parton-parton energy of $z\hat{s}$.

Therefore, after integration over the collinear gluon degrees of freedom, we obtain[9]

$$\begin{aligned} d\sigma_i^{\text{HC}} &= d\hat{\sigma}^0 \left[\frac{\alpha_s}{2\pi} \frac{\Gamma(1-\epsilon)}{\Gamma(1-2\epsilon)} \left(\frac{4\pi\mu_r^2}{\hat{s}} \right)^\epsilon \right] \left(-\frac{1}{\epsilon} \right) \delta_c^{-\epsilon} [P_{bb}(z, \epsilon) G_{b/A}(x_1/z) G_{g/B}(x_2) \right. \\ &\quad \left. + P_{gg}(z, \epsilon) G_{g/A}(x_1/z) G_{b/B}(x_2) + (x_1 \leftrightarrow x_2)] \frac{dz}{z} \left(\frac{1-z}{z} \right)^{-\epsilon} dx_1 dx_2. \right. \end{aligned} \quad (3.29)$$

In order to factorize the collinear singularity into the parton distribution function, we introduce a scale dependent parton distribution function using the $\overline{\text{MS}}$ convention:

$$G_{i/A}(x, \mu_f) = G_{i/A}(x) + \left(-\frac{1}{\epsilon} \right) \left[\frac{\alpha_s}{2\pi} \frac{\Gamma(1-\epsilon)}{\Gamma(1-2\epsilon)} \left(\frac{4\pi\mu_r^2}{\mu_f^2} \right)^\epsilon \right] \int_z^1 \frac{dz}{z} P_{ii}(z) G_{i/A}(x/z), \quad (i = b, g). \quad (3.30)$$

By using above definition, we replace $G_{g,b/A,B}$ in Eq.(3.29) and the expression for the initial state collinear contribution at $O(\alpha_s)$ order is

$$\begin{aligned} d\sigma_i^{\text{HC}} &= d\hat{\sigma}^0 \left[\frac{\alpha_s}{2\pi} \frac{\Gamma(1-\epsilon)}{\Gamma(1-2\epsilon)} \left(\frac{4\pi\mu_r^2}{\hat{s}} \right)^\epsilon \right] \{ \tilde{G}_{g/A}(x_1, \mu_f) G_{b/B}(x_2, \mu_f) + G_{g/A}(x_1, \mu_f) \tilde{G}_{b/B}(x_2, \mu_f) \right. \\ &\quad \left. + \sum_{\alpha=g,b} \left[\frac{A_1^{sc}(\alpha \rightarrow \alpha g)}{\epsilon} + A_0^{sc}(\alpha \rightarrow \alpha g) \right] G_{g/A}(x_1, \mu_f) G_{b/B}(x_2, \mu_f) + (x_1 \leftrightarrow x_2) \} dx_1 dx_2 \end{aligned} \quad (3.31)$$

where

$$\begin{aligned} A_1^{sc}(b \rightarrow bg) &= C_F(2 \ln \delta_s + 3/2), \\ A_1^{sc}(g \rightarrow gg) &= 2N \ln \delta_s + (11N - 2n_f)/6, \\ A_0^{sc} &= A_1^{sc} \ln \left(\frac{\hat{s}}{\mu_f^2} \right). \end{aligned} \quad (3.32)$$

And

$$\tilde{G}_{\alpha/A,B}(x, \mu_f) = \int_x^{1-\delta_s} \frac{dy}{y} G_{\alpha/A,B}(x/y, \mu_f) \tilde{P}_{\alpha\alpha}(y), \quad (\alpha = g, b), \quad (3.33)$$

with

$$\tilde{P}_{\alpha\alpha}(y) = P_{\alpha\alpha} \ln \left(\delta_c \frac{1-y}{y} \frac{\hat{s}}{\mu_f^2} \right) - P'_{\alpha\alpha}(y,), \quad (\alpha = g, b). \quad (3.34)$$

We can observe that the sum of the soft (Eq.(3.18)), collinear(Eq.(3.24),(3.31)), and ultraviolet renormalized virtual correction (Eq.(3.5)) terms is finite, i.e.,

$$\begin{aligned} A_2^S + A_2^V &= 0, \\ A_1^S + A_1^V + A_1^{b \rightarrow bg} + A_1^{sc}(b \rightarrow bg) + A_1^{sc}(g \rightarrow gg) &= 0. \end{aligned} \quad (3.35)$$

The final result for the $O(\alpha_s)$ correction consists of two contributions to the cross section: a two-body term $\sigma^{(2)}$ and a three-body term $\sigma^{(3)}$.

$$\begin{aligned} \sigma^{(2)} &= \frac{\alpha_s}{2\pi} \int dx_1 dx_2 d\hat{\sigma}^0 \{ G_{g/A}(x_1, \mu_f) G_{b/B}(x_2, \mu_f) [A_0^S + A_0^V + A_0^{b \rightarrow bg} + A_0^{sc}(b \rightarrow bg) + A_0^{sc}(g \rightarrow gg)] \\ &+ \tilde{G}_{g/A}(x_1, \mu_f) G_{b/B}(x_2, \mu_f) + G_{g/A}(x_1, \mu_f) \tilde{G}_{b/B}(x_2, \mu_f) + (x_1 \leftrightarrow x_2) \}. \end{aligned} \quad (3.36)$$

And

$$\sigma^{(3)} = \int dx_1 dx_2 [G_{g/A}(x_1, \mu_f) G_{b/B}(x_2, \mu_f) + (x_1 \leftrightarrow x_2)] d\hat{\sigma}^{(3)}, \quad (3.37)$$

with the hard-non-collinear partonic cross section given by

$$d\hat{\sigma}^{(3)} = \frac{1}{2\hat{s}_{12}} \int_{\text{HC}} \overline{\sum} |M_3(bg \rightarrow h^0 bg)|^2 d\Gamma_3. \quad (3.38)$$

Finally, the NLO total cross section for $pp(\text{or } p\bar{p}) \rightarrow bh^0 + X$ is

$$\sigma^{NLO} = \sigma^0 + \sigma^{(2)} + \sigma^{(3)}. \quad (3.39)$$

IV. NUMERICAL RESULTS AND DISCUSSION

In the following numerical evaluation, we present the results of the cross section for the Higgs boson production associated with a single high- p_T bottom quark via subprocess $bg(\bar{b}g) \rightarrow h^0 b(h^0 \bar{b})$ at the Fermilab Tevatron and the CERN LHC. At the LHC, the b -jet is required to have a transverse momentum cut $p_T(b) > 30\text{GeV}$ and a rapidity cut $|\eta(b)| < 2.5$. At the Tevatron, the b tagging regions are taken to be $|\eta(b)| < 2$ and $p_T(b) > 15\text{GeV}$. The SM parameters are taken as: $m_t = 174.3\text{ GeV}$, $m_Z = 91.188\text{ GeV}$, $m_W = 80.419\text{ GeV}$ and $\alpha_{EW} = 1/128$ [12]. For simplicity, the renormalization and

factorization scales are taken as $\mu_r = \mu_f = m_h$. We use the one-loop formula for the running strong coupling constant α_s with $\alpha_s(m_Z) = 0.117$.

The relevant MSSM parameters in our calculation are: the parameters $M_{\tilde{Q},\tilde{U},\tilde{D}}$ and $A_{t,b}$ in squark mass matrices, the higgsino mass parameter μ , the masses of the gluino $m_{\tilde{g}}$ and the A^0 Higgs boson m_A , the ratio of the vacuum expectation values of the two Higgs doublets $\tan \beta$. The squark mass matrix is defined as

$$\mathcal{M}_{\tilde{q}}^2 = \begin{pmatrix} m_{\tilde{q}_L}^2 & a_q m_q \\ a_q m_q & m_{\tilde{q}_R}^2 \end{pmatrix} \quad (4.1)$$

with

$$\begin{aligned} m_{\tilde{q}_L}^2 &= M_{\tilde{Q}}^2 + m_q^2 + m_Z^2 \cos 2\beta (I_3^q - e_q \sin^2 \theta_W), \\ m_{\tilde{q}_R}^2 &= M_{\{\tilde{U},\tilde{D}\}}^2 + m_q^2 + m_Z^2 \cos 2\beta e_q \sin^2 \theta_W \\ a_q &= A_q - \mu \{\cot \beta, \tan \beta\}, \end{aligned} \quad (4.2)$$

for $\{\text{up, down}\}$ type squarks. I_3^q and e_q are the third component of the weak isospin and the electric charge of the quark q . The chiral states \tilde{q}_L and \tilde{q}_R are transformed into the mass eigenstates \tilde{q}_1 and \tilde{q}_2 :

$$\begin{pmatrix} \tilde{q}_1 \\ \tilde{q}_2 \end{pmatrix} = R^{\tilde{q}} \begin{pmatrix} \tilde{q}_L \\ \tilde{q}_R \end{pmatrix}, \quad R^{\tilde{q}} = \begin{pmatrix} \cos \theta_{\tilde{q}} & \sin \theta_{\tilde{q}} \\ -\sin \theta_{\tilde{q}} & \cos \theta_{\tilde{q}} \end{pmatrix}. \quad (4.3)$$

Then the mass eigenvalues $m_{\tilde{q}_1}$ and $m_{\tilde{q}_2}$ are given by

$$\begin{pmatrix} m_{\tilde{q}_1}^2 & 0 \\ 0 & m_{\tilde{q}_2}^2 \end{pmatrix} = R^{\tilde{q}} \mathcal{M}_{\tilde{q}}^2 (R^{\tilde{q}})^\dagger \quad (4.4)$$

For simplicity, we assume $M_{\tilde{Q}} = M_{\tilde{U}} = M_{\tilde{D}} = A_t = A_b = 600 \text{ GeV}$, $\mu = 200 \text{ GeV}$, and $m_A = m_{\tilde{g}} = 200 \text{ GeV}$ by default unless otherwise stated.

In our calculation, we use the program FeynHiggsFast [13] to generate the mass of Higgs boson(h^0) and the mixing angle α , and use the CTEQ5L parton distribution functions[14]. The $\overline{\text{MS}}$ bottom quark mass \overline{m}_b can be evaluated by using the next-leading order formula [15]. In the following equations, we use $\overline{m}_b(Q)$ to denote the $\overline{\text{MS}}$ bottom quark mass.

$$\overline{m}_b(Q) = U_5(Q, \overline{m}_b) \overline{m}_b(\overline{m}_b), \quad \text{for } Q < m_t,$$

$$\overline{m}_b(Q) = U_6(Q, m_t) U_5(m_t, \overline{m}_b) \overline{m}_b(\overline{m}_b), \quad \text{for } Q > m_t, \quad (4.5)$$

where $\overline{m}_b = \overline{m}_b(\overline{m}_b) = 4.3 \text{ GeV}$. The evolution factor $U_f(f = 5, 6)$ is

$$U_f(Q_2, Q_1) = \left(\frac{\alpha_s(Q_2)}{\alpha_s(Q_1)} \right)^{d^{(f)}} \left[1 + \frac{\alpha_s(Q_1) - \alpha_s(Q_2)}{4\pi} J^{(f)} \right],$$

$$d^{(f)} = \frac{12}{33 - 2f}, \quad J^{(f)} = -\frac{8982 - 504f + 40f^2}{3(33 - 2f)^2} \quad (4.6)$$

In addition, we also improve the perturbative calculations through the following replacement[15]

$$\overline{m}_b(Q) \rightarrow \frac{\overline{m}_b(Q)}{1 + \Delta m_b}, \quad (4.7)$$

where

$$\Delta m_b = \frac{2\alpha_s}{3\pi} m_{\tilde{g}} \tan \beta I(m_{\tilde{b}_1}, m_{\tilde{b}_2}, m_{\tilde{g}}), \quad (4.8)$$

with

$$I(a, b, c) = \frac{1}{(a^2 - b^2)(b^2 - c^2)(a^2 - c^2)} (a^2 b^2 \log \frac{a^2}{b^2} + b^2 c^2 \log \frac{b^2}{c^2} + c^2 a^2 \log \frac{c^2}{a^2}). \quad (4.9)$$

Fig.6 shows that our NLO-QCD result does not depend on the arbitrary cutoffs δ_s and δ_c by using the two cutoff phase space slicing method. The two-body($\sigma^{(2)}$) and three-body($\sigma^{(3)}$) contributions and the NLO cross section (σ^{NLO}) are shown as a function of the soft cutoff δ_s with the collinear cutoff $\delta_c = \delta_s/50$, and $\tan \beta = 4$. We can see the NLO cross section σ^{NLO} is independent of the cutoffs. In the following numerical calculations, we take $\delta_s = 10^{-5}$ and $\delta_c = \delta_s/50$.

Fig.7 shows the dependence of the relative NLO-QCD corrections of the process $pp(\text{or } p\bar{p}) \rightarrow bg(\bar{b}g) \rightarrow h^0 b(h^0 \bar{b}) + X$ on the mass of A^0 Higgs boson m_A at the LHC. There we take $\tan \beta = 10, 40$ and define the relative correction as

$$\Delta = \frac{\sigma^{NLO} - \sigma^0}{\sigma^0}. \quad (4.10)$$

For $\tan \beta = 10$, the relative NLO-QCD correction is about 58% to 60%. And for $\tan \beta = 40$, the relative NLO-QCD correction increases from 66.5% to 73.5% with the increment of m_A from 200 GeV to 800 GeV.

To compare the production cross section of the processes pp (or $p\bar{p}$) $\rightarrow bg(\bar{b}g) \rightarrow h^0b(h^0\bar{b}) + X$ in the MSSM with the corresponding cross section in the SM, we introduce the ratio of σ_{MSSM} and σ_{SM} . The cross section σ_{MSSM} in the MSSM and the corresponding σ_{SM} in the SM including one-loop order QCD corrections, can be expressed as

$$\begin{aligned}\sigma_{MSSM} &= \sigma_{MSSM}^0(1 + \Delta_{MSSM}) \\ \sigma_{SM} &= \sigma_{SM}^0(1 + \Delta_{SM}).\end{aligned}\quad (4.11)$$

In Fig.8, we depict the dependence of the ratio $\sigma_{MSSM}/\sigma_{SM}$ on A^0 Higgs boson mass m_A at the Tevatron. We see that the ratio $\sigma_{MSSM}/\sigma_{SM}$ decreases with the increment of m_A . When m_A is in the range between $200 - 300$ GeV, the cross section of the process $p\bar{p} \rightarrow bg(\bar{b}g) \rightarrow h^0b(h^0\bar{b}) + X$ in the MSSM at the Tevatron is greatly enhanced over that in the SM, but when m_A increases from 300 GeV to 800 GeV, the differences of the SM and the MSSM cross section is becoming smaller. That is because in the MSSM parameter space for $m_A = 200 - 300$ GeV, the coupling factor between Higgs boson h^0 and bottom quarks $\sin \alpha/\cos \beta > 1$, while in the region of $m_A > 300$ GeV, the value of $\sin \alpha/\cos \beta$ is getting close to 1.

Fig.9 shows the cross sections of the process $pp \rightarrow bg(\bar{b}g) \rightarrow h^0b(h^0\bar{b}) + X$ at the LHC and $p\bar{p} \rightarrow bg(\bar{b}g) \rightarrow h^0b(h^0\bar{b}) + X$ at the Tevatron as the functions of $\tan \beta$. We scale the mass of the Higgs boson m_h under the X-axis to show the changes of the phase space with $\tan \beta$. The figure shows that when $\tan \beta$ varies from 5 to 10, the cross sections drop quickly and m_{h^0} increases faster than in other $\tan \beta$ regions. But when $\tan \beta$ is larger than 10, the variation of mass of Higgs boson(h^0) is not sensitive to $\tan \beta$, and the cross sections drop smoothly with the increasing of $\tan \beta$. When $\tan \beta$ approaches to the value of 50, the relative NLO-QCD corrections take the value about 70% at the LHC and 85% at the Tevatron. The curve behavior shown in Fig.9, comes from the feature of the phase space variation versus $\tan \beta$. In Fig.10 we present the dependence of $\sigma_{MSSM}/\sigma_{SM}$ on $\tan \beta$ at the LHC and Tevatron. We find that the cross section of the processes pp (or $p\bar{p}$) $\rightarrow bg(\bar{b}g) \rightarrow h^0b(h^0\bar{b}) + X$ in the MSSM is greatly enhanced compared with that in the SM in all the plotted range of $\tan \beta = 4 \sim 50$

with the parameter space we take. That is due to the stronger coupling strength between Higgs boson h^0 and bottom quarks with large $\tan\beta$ in the MSSM than in the SM. Then the production of the processes $pp(\text{or } p\bar{p}) \rightarrow h^0 b(h^0 \bar{b}) + X$ at hadron colliders could be enhanced significantly in the MSSM.

To study the decoupling behavior of SUSY QCD correction, we assume all SUSY mass related parameters have the same quantity and are pushed to a large value except μ is taken to be 200GeV . We denote $M_{\tilde{Q}} = M_{\tilde{U}} = M_{\tilde{D}} = A_t = A_b = m_A = m_{\tilde{g}}$ collectively by M_s and define the relative SUSY QCD correction as

$$\Delta_{SQCD} = \frac{\delta\sigma^{SQCD}}{\sigma^0}, \quad (4.12)$$

where $\delta\sigma^{SQCD}$ is the cross section correction contributed by the SUSY QCD diagrams shown in Fig.3. In the mass region of $m_A = M_s > 500\text{ GeV}$, $\sin\alpha/\cos\beta$ is close to 1. Therefore, with this parameter choice, the dependence of $\Delta\sigma_{SQCD}$ on M_s can demonstrate the decoupling behavior of SUSY QCD correction in the processes $pp(\text{or } p\bar{p}) \rightarrow h^0 b(h^0 \bar{b}) + X$ at hadron colliders. In Fig.11, we depict the relative SUSY QCD correction Δ_{SQCD} as the functions of M_s at the LHC. From the figure, we can see that for $\tan\beta = 10$ the relative SUSY QCD correction is approaching to zero with M_s increasing to 2.2 TeV , but for $\tan\beta = 40$ the relative correction decreases to about 4% with M_s increasing to 3 TeV . That shows obviously that the large $\tan\beta$ enhances the SUSY QCD corrections and delays the decoupling feature.

To analyze the scale dependence of the cross sections, we introduce the ratio of the cross section at scale Q to the cross section at scale $Q = m_{h^0}$ and depict the $\sigma(Q)/\sigma(Q = m_{h^0})$ as a function of Q/m_{h^0} at the Tevatron in Fig.12. The scale variation of the NLO-QCD cross section may be serves as an estimate of the remaining theoretical uncertainty of the high order corrections. Fig.12 shows that it is evident that the one-loop NLO-QCD corrections reduce the LO scale dependence.

In summary, we have computed the production of Higgs boson h^0 associated with a single high- p_T bottom quark via subprocess $bg(\bar{b}g) \rightarrow h^0 b(h^0 \bar{b})$ including the NLO-QCD corrections in the MSSM at the CERN LHC and the Fermilab Tevatron. We find that due to the enhancement of the Yukawa couplings strength of the down-type quarks with Higgs bosons at large $\tan\beta$, the cross section of the

$pp \rightarrow h^0 b(h^0 \bar{b})$ can reach hundreds of fermi barn at the LHC and the cross section of the $p\bar{p} \rightarrow h^0 b(h^0 \bar{b})$ can reach dozens of fermi barn at the Tevatron. The NLO-QCD correction reaches $50\% \sim 70\%$ at the LHC and $60\% \sim 85\%$ at the Tevatron in the parameter space we have chosen.

Acknowledgments: The authors are very grateful to Prof. T. Han and Dr. Wan Lang-Hui for their encouragement and the useful discussions. This work was supported in part by the National Natural Science Foundation of China and a grant from the University of Science and Technology of China.

Appendix A

In Appendix A, we list the explicit expressions of the renormalization constants. By using the $\overline{\text{MS}}$ scheme the renormalization constants defined in Eq.(3.1) are expressed as:

$$\begin{aligned}\delta Z_b &= -\frac{\alpha_s}{4\pi} C_F \Delta, \\ \frac{\delta m_b}{m_b} &= -\frac{\alpha_s}{2\pi} C_F \Delta, \\ \delta Z_g &= -\frac{\alpha_s}{4\pi} \left(\frac{1}{2}N - \frac{1}{2}\beta_0\right) \Delta,\end{aligned}\tag{A.1}$$

where $\Delta = \frac{1}{\epsilon} - \gamma_E + \log(4\pi)$, $\beta_0 = (11N - 2n_f)/3$, $N = 3$ and $C_F = 4/3$.

We define the following symbols

$$\begin{aligned}C_{gb\bar{b}} &= \frac{1}{2}\delta Z_g + \delta Z_b + \delta Z_{g_s}, \\ C_{hb\bar{b}} &= \delta Z_b + \delta Y_b, \quad C_{b\bar{b}} = \delta Z_b.\end{aligned}\tag{A.2}$$

Then the amplitude from the diagrams which contain counter terms M^{CT} can be written as

$$\begin{aligned}M^{CT} &= \frac{g_s Y_b}{\hat{s}^2} \bar{u}_i(k_4) [\hat{s}(C_{gb\bar{b}} + C_{hb\bar{b}})(\not{p}_1 + \not{p}_2) - C_{b\bar{b}}(\not{p}_1 + \not{p}_2)^2] \gamma_\mu u_j(p_1) \epsilon_\mu(p_2) T_{ij}^a \\ &+ \frac{g_s Y_b}{\hat{t}^2} \bar{u}_i(k_4) [\hat{t}(C_{gb\bar{b}} + C_{hb\bar{b}})(\not{p}_1 - \not{k}_3) - C_{b\bar{b}}(\not{p}_1 - \not{k}_3)^2] \gamma_\mu u_j(p_1) \epsilon_\mu(p_2) T_{ij}^a.\end{aligned}\tag{A.3}$$

Appendix B

In Appendix B, we present expressions of the non-vanishing form factors in Eq.(3.3). We denote the couplings between gluino, quark and squark as

$$\tilde{g} - \tilde{t}_i - \bar{t} : (V_{\tilde{g}\tilde{t}_i t}^{(1)} P_L + V_{\tilde{g}\tilde{t}_i t}^{(2)} P_R) T^a, \quad \tilde{g} - \tilde{b}_i - \bar{b} : (V_{\tilde{g}\tilde{b}_i b}^{(1)} P_L + V_{\tilde{g}\tilde{b}_i b}^{(2)} P_R) T^a, \quad (\text{B.1})$$

where

$$\begin{aligned} V_{\tilde{g}\tilde{t}_1 t, \tilde{g}\tilde{b}_1 b}^{(1)} &= -i\sqrt{2}g_s \sin \theta_{\tilde{t}, \tilde{b}}, & V_{\tilde{g}\tilde{t}_2 t, \tilde{g}\tilde{b}_2 b}^{(1)} &= i\sqrt{2}g_s \cos \theta_{\tilde{t}, \tilde{b}}, \\ V_{\tilde{g}\tilde{t}_1 t, \tilde{g}\tilde{b}_1 b}^{(2)} &= -i\sqrt{2}g_s \cos \theta_{\tilde{t}, \tilde{b}}, & V_{\tilde{g}\tilde{t}_2 t, \tilde{g}\tilde{b}_2 b}^{(2)} &= -i\sqrt{2}g_s \sin \theta_{\tilde{t}, \tilde{b}}. \end{aligned} \quad (\text{B.2})$$

And the couplings between the Higgs boson and two quarks(squarks) are denoted as

$$h - b - \bar{b} : V_{hbb}, \quad h - \tilde{b}_i - \tilde{b}_j^\dagger : V_{h\tilde{b}_i \tilde{b}_j}, \quad h - \tilde{t}_i - \tilde{t}_j^\dagger : V_{h\tilde{t}_i \tilde{t}_j}, \quad (\text{B.3})$$

where the explicit expressions of the V_{hbb} , $V_{h\tilde{b}_i \tilde{b}_j}$ and $V_{h\tilde{t}_i \tilde{t}_j}$ can be found in Ref.[16]. For simplicity, we introduce the following abbreviations,

$$\begin{aligned} V_{\tilde{g}\tilde{b}_i b}^{(1)*} \cdot V_{\tilde{g}\tilde{b}_j b}^{(1)} &= F_{ij}^1, & V_{\tilde{g}\tilde{b}_i b}^{(1)*} \cdot V_{\tilde{g}\tilde{b}_j b}^{(2)} &= F_{ij}^2, \\ V_{\tilde{g}\tilde{b}_i b}^{(2)*} \cdot V_{\tilde{g}\tilde{b}_j b}^{(1)} &= F_{ij}^3, & V_{\tilde{g}\tilde{b}_i b}^{(2)*} \cdot V_{\tilde{g}\tilde{b}_j b}^{(2)} &= F_{ij}^4, \end{aligned} \quad (\text{B.4})$$

and

$$\begin{aligned} B_0^a, B_1^a &= B_0, B_1[p_1, 0, 0], & B_0^b, B_1^b &= B_0, B_1[k_3 - p_1, 0, 0], \\ B_0^c, B_1^c &= B_0, B_1[-p_1 - p_2, 0, 0], & B_0^d, B_1^d &= B_0, B_1[k_3 - p_1, m_{\tilde{g}}, m_{\tilde{b}_i}], \\ B_0^e, B_1^e &= B_0, B_1[-p_1 - p_2, m_{\tilde{b}_i}, m_{\tilde{g}}], & C_0^a, C_{kl}^a &= C_0, C_{kl}[-k_3, p_1, 0, 0, 0], \\ C_0^b, C_{kl}^b &= C_0, C_{kl}[-p_2, -p_1, 0, 0, 0], & C_0^c, C_{kl}^c &= C_0, C_{kl}[-p_2, k_3 - p_1, 0, 0, 0], \\ C_0^d, C_{kl}^d &= C_0, C_{kl}[k_3, -p_1 - p_2, 0, 0, 0], & C_0^e, C_{kl}^e &= C_0, C_{kl}[-k_3, p_1, m_{\tilde{b}_j}, m_{\tilde{b}_i}, m_{\tilde{g}}], \\ C_0^f, C_{kl}^f &= C_0, C_{kl}[-p_2, -p_1, m_{\tilde{g}}, m_{\tilde{b}_i}], & C_0^g, C_{kl}^g &= C_0, C_{kl}[-p_2, -p_1, m_{\tilde{b}_i}, m_{\tilde{b}_i}, m_{\tilde{g}}], \\ C_0^h, C_{kl}^h &= C_0, C_{kl}[-p_2, k_3 - p_1, m_{\tilde{g}}, m_{\tilde{b}_i}], & C_0^m, C_{kl}^m &= C_0, C_{kl}[-p_2, k_3 - p_1, m_{\tilde{b}_i}, m_{\tilde{b}_i}, m_{\tilde{g}}], \\ C_0^n, C_{kl}^n &= C_0, C_{kl}[k_3, -p_1 - p_2, m_{\tilde{b}_j}, m_{\tilde{b}_i}, m_{\tilde{g}}], & D_0^a, D_{kl}^a &= D_0, D_{kl}[-p_2, k_3, -p_1, 0, 0, 0, 0], \\ D_0^b, D_{kl}^b &= D_0, D_{kl}[-p_2, k_3, -p_1, m_{\tilde{b}_j}, m_{\tilde{b}_i}, m_{\tilde{b}_i}, m_{\tilde{g}}], \\ D_0^c, D_{kl}^c &= D_0, D_{kl}[k_3, -p_1, -p_2, m_{\tilde{b}_j}, m_{\tilde{b}_i}, m_{\tilde{g}}, m_{\tilde{g}}] \end{aligned} \quad (\text{B.5})$$

Since we neglect the bottom quark mass throughout the calculation except in the Yukawa couplings, the form factors $f_{1,2,7,8,9,10}$ are irrelevant to our results and we do not present them here.

For diagrams shown in Fig.2(SM-like QCD corrections), we can write the form factors as

$$\begin{aligned} f_3 &= f_4 = \frac{3g_s V_{hbb}}{16\pi^2} [C_{22}^c - C_{23}^c + (D_{12}^a - 2D_{11}^a - 2D_{21}^a + D_{24}^a)m_h^2 + (D_{13}^a + D_{25}^a)\hat{s} \\ &\quad - (D_{12}^a - D_{13}^a + D_{24}^a - D_{25}^b)\hat{t}] \end{aligned} \quad (\text{B.6})$$

$$\begin{aligned} f_5 &= f_6 = \frac{-g_s V_{hbb}}{96\pi^2 \hat{t}} [26 + 4B_0^b - 32B_0^a - 16B_1^b - 120C_{24}^c + 16(2C_{11}^a - C_{12}^a)m_h^2 \\ &\quad + (2C_{11}^a - 9C_0^c - 4C_0^a - 18C_{11}^c + 9C_{12}^c + 16C_{12}^a + 40C_{22}^c - 40C_{23}^c + 74D_{27}^a)\hat{t} \\ &\quad + (18D_{12}^a - 29D_{11}^a + 2D_{13}^a - 29D_{21}^a - 6D_{22}^a + 18D_{24}^a + 2D_{25}^a + 4D_{26}^a)m_h^2\hat{t} \\ &\quad + (16D_{13}^a - 16D_{12}^a + 2D_{22}^a + 6D_{24}^b + 16D_{25}^a - 13D_{26}^a)\hat{s}\hat{t} \\ &\quad + (16D_{13}^a - 16D_{12}^a + 2D_{22}^a + 4D_{24}^a - 16D_{24}^a + 16D_{25}^a - 4D_{26}^a)\hat{t}^2] \end{aligned} \quad (\text{B.7})$$

$$\begin{aligned} f_{11} &= f_{12} = \frac{g_s V_{hbb}}{192\pi^2 \hat{s}} [(24 - 32B_0^c - 16B_1^c - 104C_{24}^b + 16(2C_{11}^d - C_{12}^d)m_h^2)(1 + \hat{s}/\hat{t}) \\ &\quad + (16D_{13}^a - 18D_{12}^a - 2D_{13}^a + 9D_{23}^a + 9D_{25}^a - 18D_{26}^a)\hat{s} \\ &\quad + (18C_0^b - 18C_0^c - 9C_{11}^c + 9C_{11}^b - 7C_{12}^c - 16C_{12}^d + 16C_{12}^a + 16C_{22}^c - 16C_{23}^c + 16C_{23}^b + 54D_{27}^a) \\ &\quad + (36D_{12}^a - 27D_{11}^a - 5D_{13}^a + 9D_{24}^a - 18D_{25}^a + 9D_{26}^a)m_h^2 \\ &\quad + (16D_{13}^a - 36D_{12}^a - 2D_{13}^a + 9D_{23}^a - 9D_{24}^a + 9D_{25}^a - 9D_{26}^a)\hat{t}] \end{aligned} \quad (\text{B.8})$$

For diagrams shown in Fig.3(SUSY QCD corrections), we can write the form factors as, (The summation over the particle indices of squark ($i, j = 1, 2$) has been omitted.)

$$\begin{aligned} f_3 &= \frac{g_s}{96\pi^2} [(-C_{22}^m + C_{23}^m)F_{ii}^4 V_{hbb} + (D_0^b + D_{11}^b + D_{12}^b)m_{\tilde{g}} F_{ji}^3 V_{h\tilde{b}_j \tilde{b}_i}] \\ f_4 &= f_3(F_{ii}^4 \rightarrow F_{ii}^1 \quad F_{ji}^3 \rightarrow F_{ji}^2) \\ f_5 &= \frac{g_s}{96\pi^3 \hat{t}} [(B_0^d - 8B_1^d - 18C_{24}^h - 2C_{24}^m + (9C_{22}^h + C_{22}^m - 9C_{23}^h - C_{23}^m)\hat{t})F_{ii}^4 V_{hbb} \\ &\quad + (8C_0^e - (D_0^b + 9D_0^c + D_{11}^b + 9D_{11}^c + D_{12}^c)\hat{t})m_{\tilde{g}} F_{ji}^3 V_{h\tilde{b}_j \tilde{b}_i}] \\ f_6 &= f_5(F_{ii}^4 \rightarrow F_{ii}^1 \quad F_{ji}^3 \rightarrow F_{ji}^2) \end{aligned}$$

$$\begin{aligned}
f_{11} &= \frac{g_s}{384\pi^2\hat{s}\hat{t}}[\hat{t}(9 + 16B_0^e + 16B_1^e - 36C_{24}^f + 4C_{24}^g + 18C_{12}^f\hat{s} + 18C_{23}^f\hat{s} - 18C_0^f m_{\tilde{g}}^2)F_{ii}^1 V_{hbb} \\
&+ \hat{s}(9 + 16B_0^d + 16B_1^d - 36C_{24}^h + 4C_{24}^i + 18C_{22}^h\hat{t} - 18C_{23}^h\hat{t} - 18C_0^h m_{\tilde{g}}^2)F_{ii}^4 V_{hbb} \\
&- 2(8C_0^e\hat{s} + 8C_0^n\hat{t} - 9D_0^c\hat{s}\hat{t})m_{\tilde{g}}F_{ji}^3 V_{h\tilde{b}_j\tilde{b}_i}] \\
f_{12} &= f_{11}(F_{ii}^4 \leftrightarrow F_{ii}^1 \quad F_{ji}^3 \leftrightarrow F_{ji}^2) \tag{B.9}
\end{aligned}$$

In our paper we adopt the definitions of the one-loop integrals in Ref. [17]. The numerical calculation of the vector and tensor one-loop integral functions can be traced back to four scalar loop integrals A_0 , B_0 , C_0 , D_0 as shown in Ref.[18]. Many of the integral functions contain the soft and collinear IR singularities, the formulas to calculate these integrals can be found in Ref. [19].

References

- [1] S. Weinberg, Phys. Rev. Lett. **19**, 1264 (1967); S. Glashow, Nucl. Phys. **B22**, 579 (1961); A. Salam, in *Elementary Particle Theory*, edited by N. Svartholm, (1968) p367.
- [2] H. P. Nilles Phys. Rep. **110**, 1 (1984); H. E. Haber and G. L. Kane, Phys. Rep. **117**, 75 (1985).
- [3] J. F. Gunion, H. E. Haber, Nucl. Phys. **B272**, 1 (1986).
- [4] A. Stange, W. Marciano and S. Willenbrock, Phys. Rev. **D49**, 1354 (1994).
- [5] D.A. Dicus and S. Willenbrock, Phys. Rev. **D39**, 751 (1989).
- [6] C.S. Huang and S. H. Zhu, Phys. Rev. D **60**, 075012 (1999).
- [7] J. Campbell, R.K. Ellis, F. Maltoni and S. Willenbrock, Phys. Rev. D **67**, 095002 (2003).
- [8] M.A.G. Aivazis, J.C. Collins, F.I. Olness, and W.K. Tung, Phys. Rev. D **50** 3102 (1994); J.C. Collins, Phys. Rev. D **58** 094002 (1998); M. Kramer, F.I. Olness, D.E. Soper, Phys. Rev. D **62** 096007 (2000);
- [9] B.W. Harris and J.F. Owens, Phys. Rev. D **65** 094032(2002)

[10] G.P. Lepage, J. Comput. Phys. **27**, 192(1978)

[11] G. Altarelli and G. Parisi, Nucl. Phys. **B126** 298 (1977)

[12] Particle Data Group, Eur. Phys. J. **C15** 2000.

[13] S. Heinemeyer, W. Hollik and G. Weiglein, CERN-TH/2000-55, DESY 00-020, KA-TP-3-2000, arXiv:hep-ph/0002213.

[14] H. L. Lai *et al.* [CTEQ Collaboration], Eur. Phys. J. **C12**, 375(2000).

[15] M. Carena, D. Garcia, U. Nierste and C.E. Wagner, Nucl. Phys. **B577**, 88 (2000).

[16] M.L. Zhou, W.G. Ma, L. Han, Y. Jian and H. Zhou, J. Phys. **G25**, 1641 (1999).

[17] Bernd A. Kniehl, Phys. Rep. **240**, 211 (1994).

[18] G. Passarino and M. Veltman, Nucl. Phys. **B160**, 151 (1979).

[19] W. Beenakker, H. Kuijf, W.L. van Neerven and J. Smith, Phys. Rev. **D40**, 54 (1989)

Figure Captions

Fig.1 Leading order Feynman diagrams for the subprocess of $bg \rightarrow h^0b$.

Fig.2 Virtual one-loop Feynman diagrams of the SM-like QCD corrections.

Fig.3 Virtual one-loop Feynman diagrams of the SUSY QCD corrections.

Fig.4 Feynman diagrams that contain counter-term.

Fig.5 Feynman diagrams for the real gluon emission.

Fig.6 Dependence of the cross sections for the h^0b production at the Tevatron on the cutoff δ_s with $\delta_c = \delta_s/50$.

Fig.7 The dependence of the relative NLO-QCD correction on the m_A with $\tan \beta = 4, 10$ at the LHC.

Fig.8 The dependence of $\sigma_{MSSM}/\sigma_{SM}$ on the m_A with $\tan \beta = 4, 10$ at the Tevatron.

Fig.9 The dependence of the cross sections on $\tan \beta$ at the LHC and the Tevatron.

Fig.10 The dependence of $\sigma_{MSSM}/\sigma_{SM}$ on $\tan \beta$ at the LHC and the Tevatron.

Fig.11 The dependence of Δ_{SQCD} on M_s at the LHC.

Fig.12 The variation of the $\sigma(Q)/\sigma(Q = m_{h^0})$ with the ratio Q/m_{h^0} at the Tevatron.

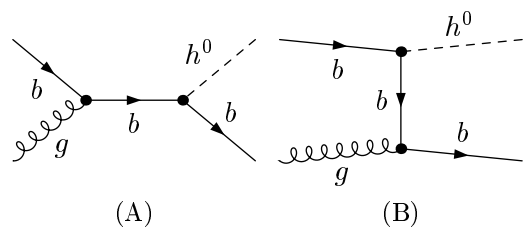


Fig.1

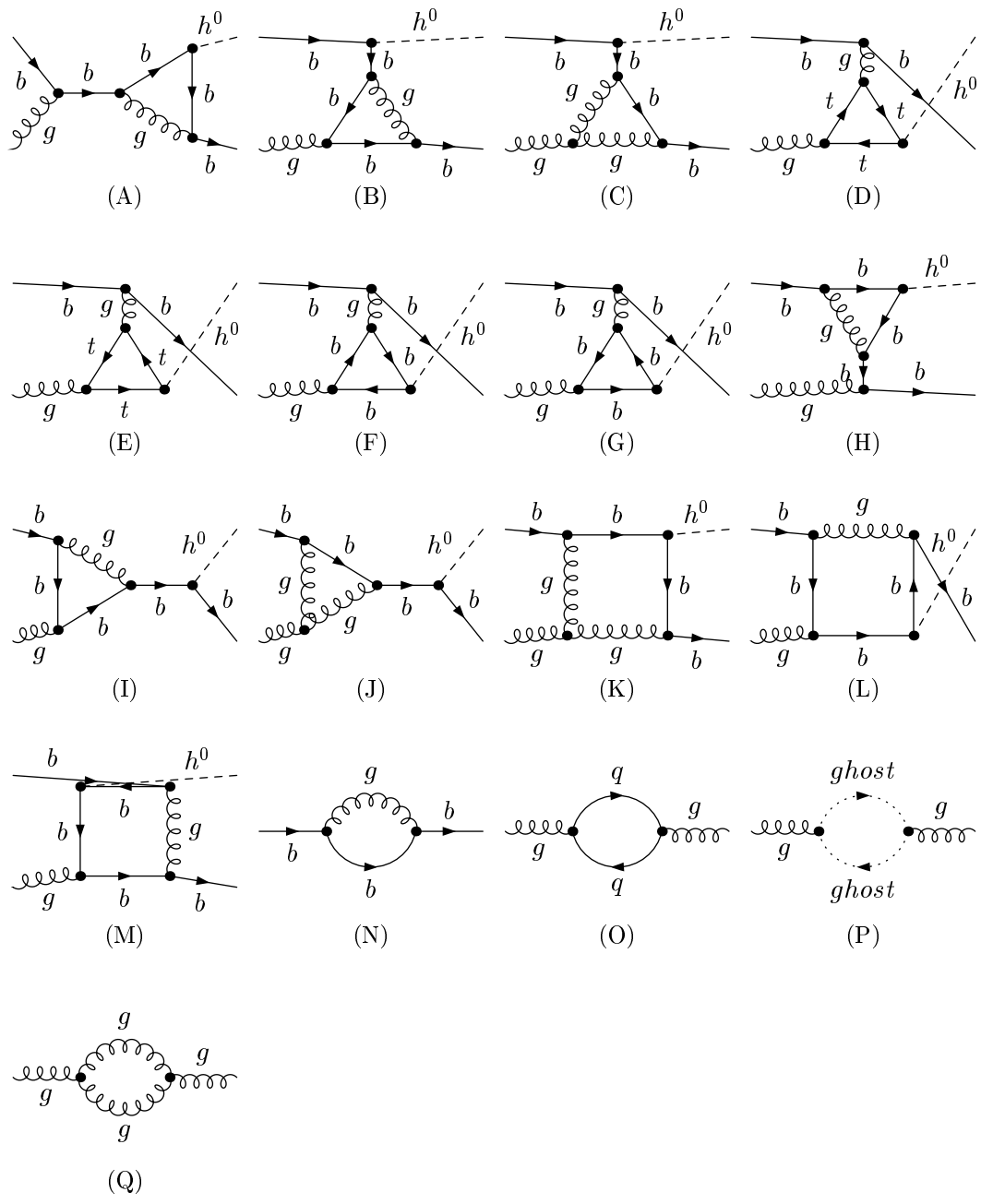


Fig.2

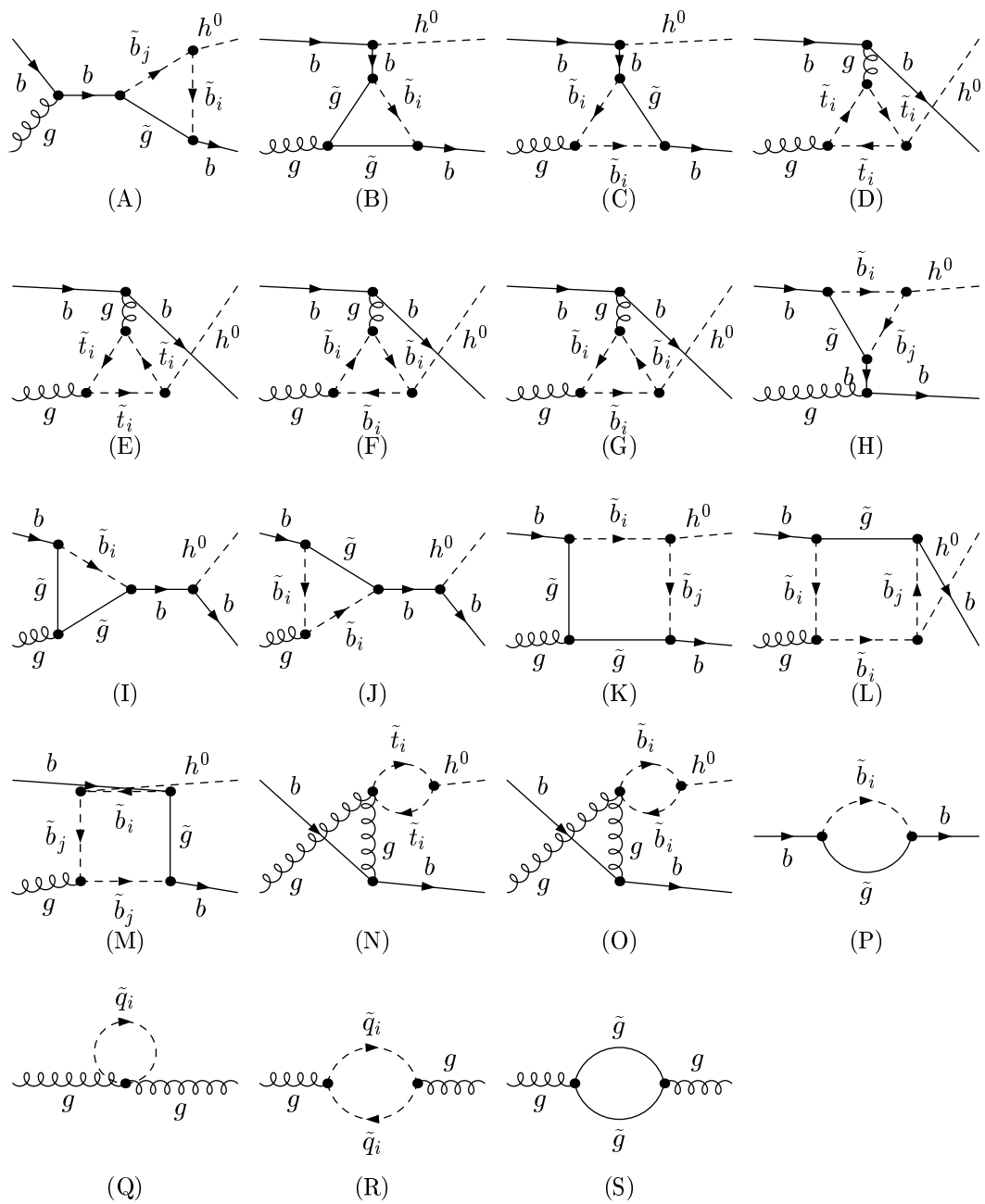


Fig.3

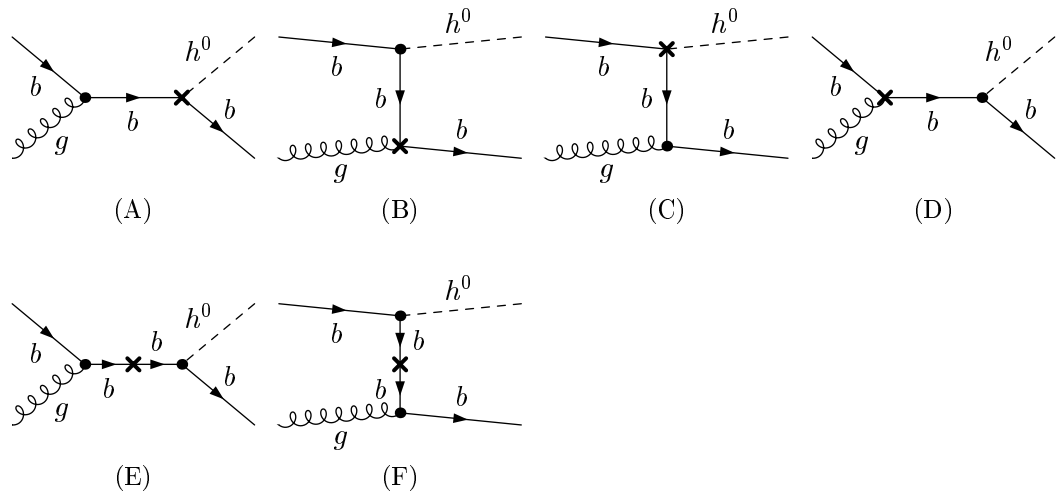


Fig.4

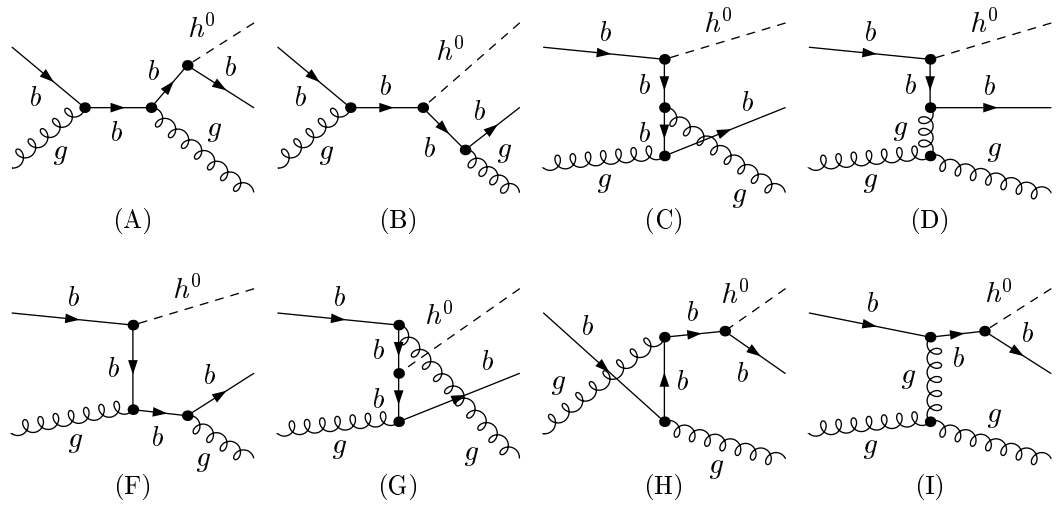


Fig.5

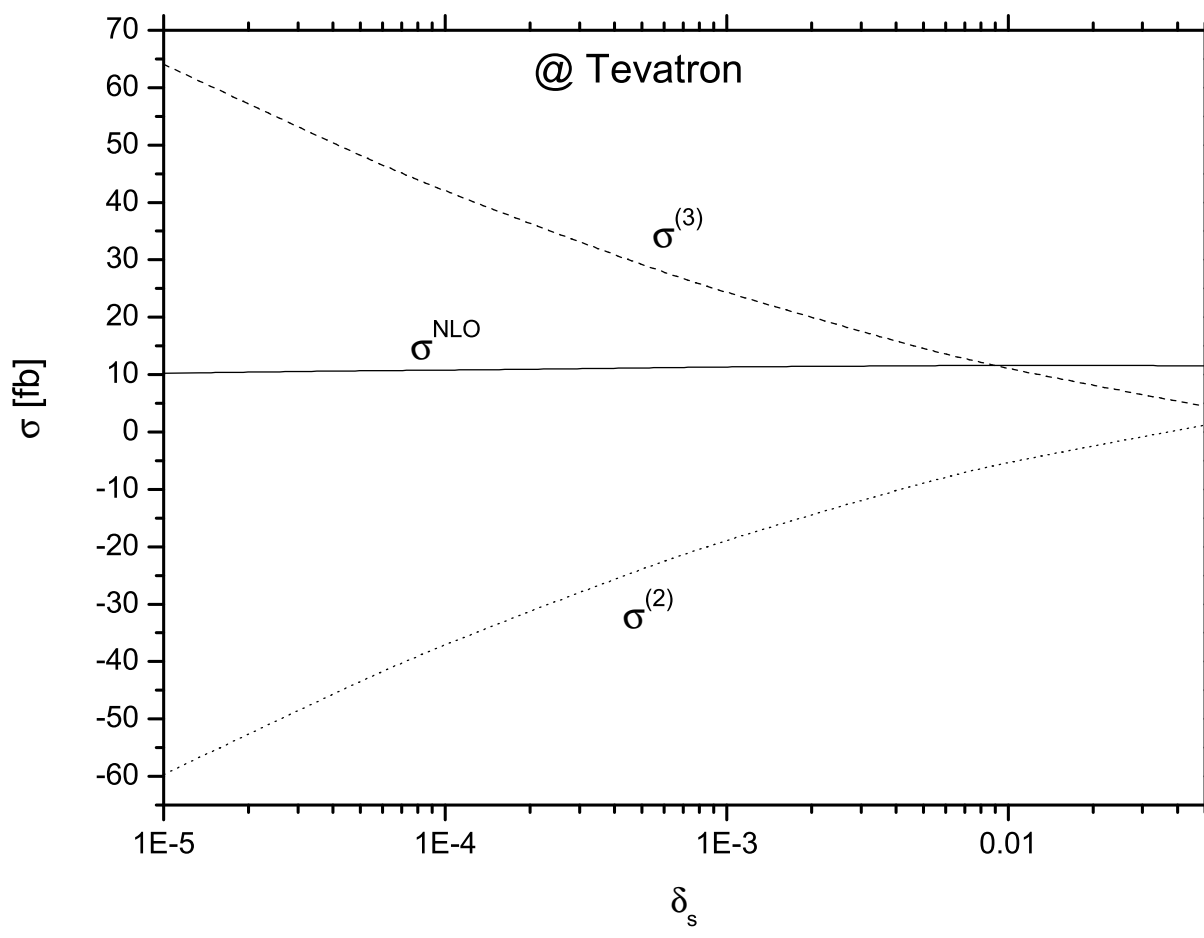


Fig.6

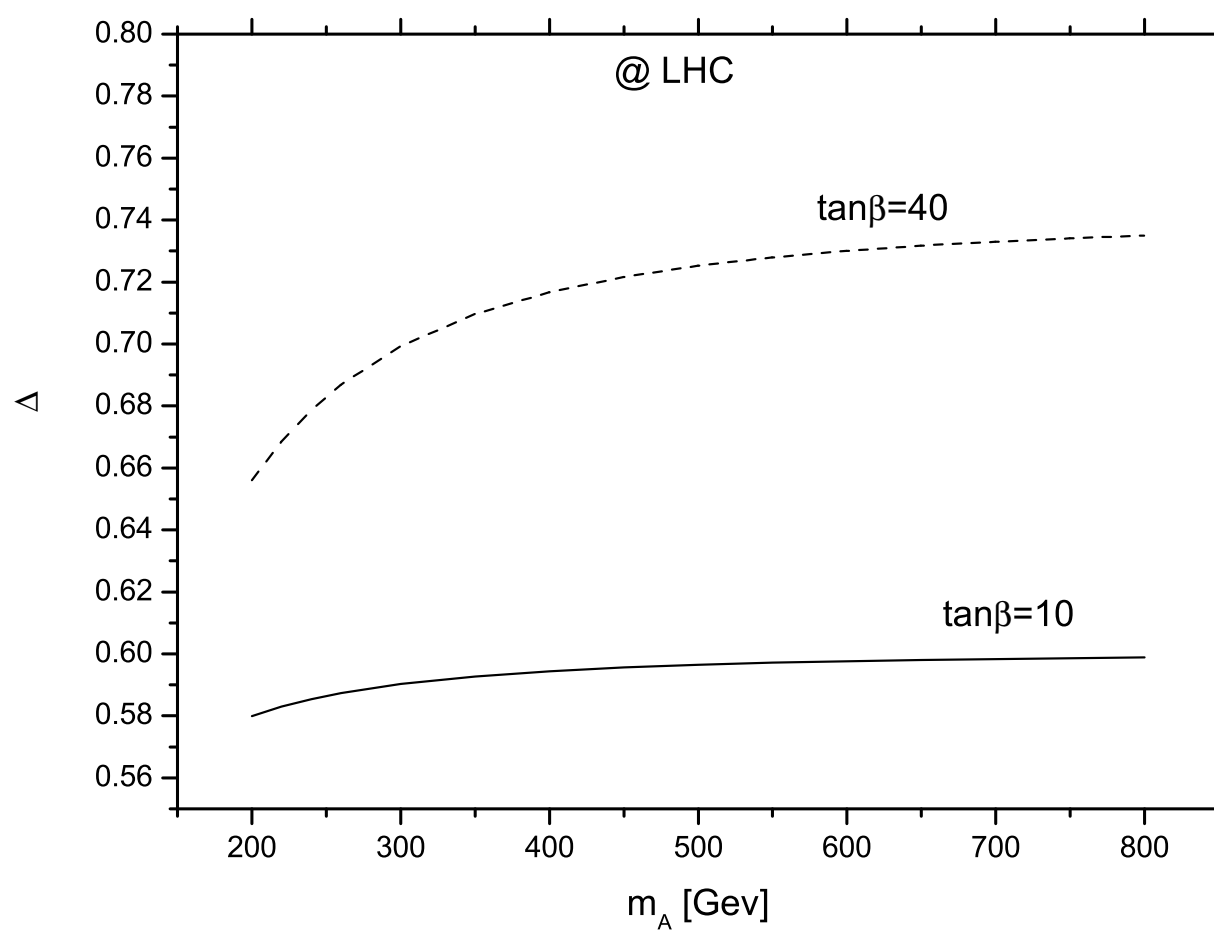


Fig.7

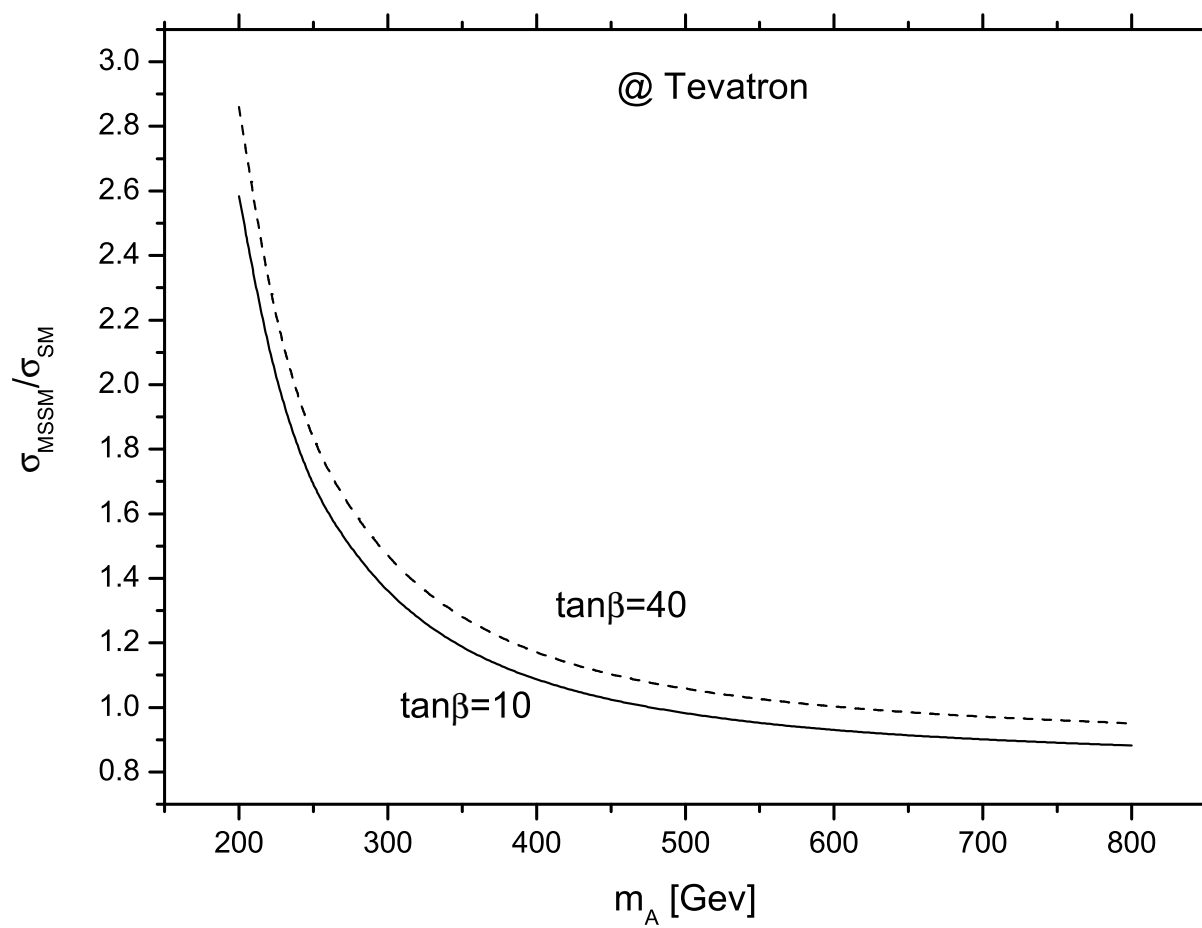


Fig.8

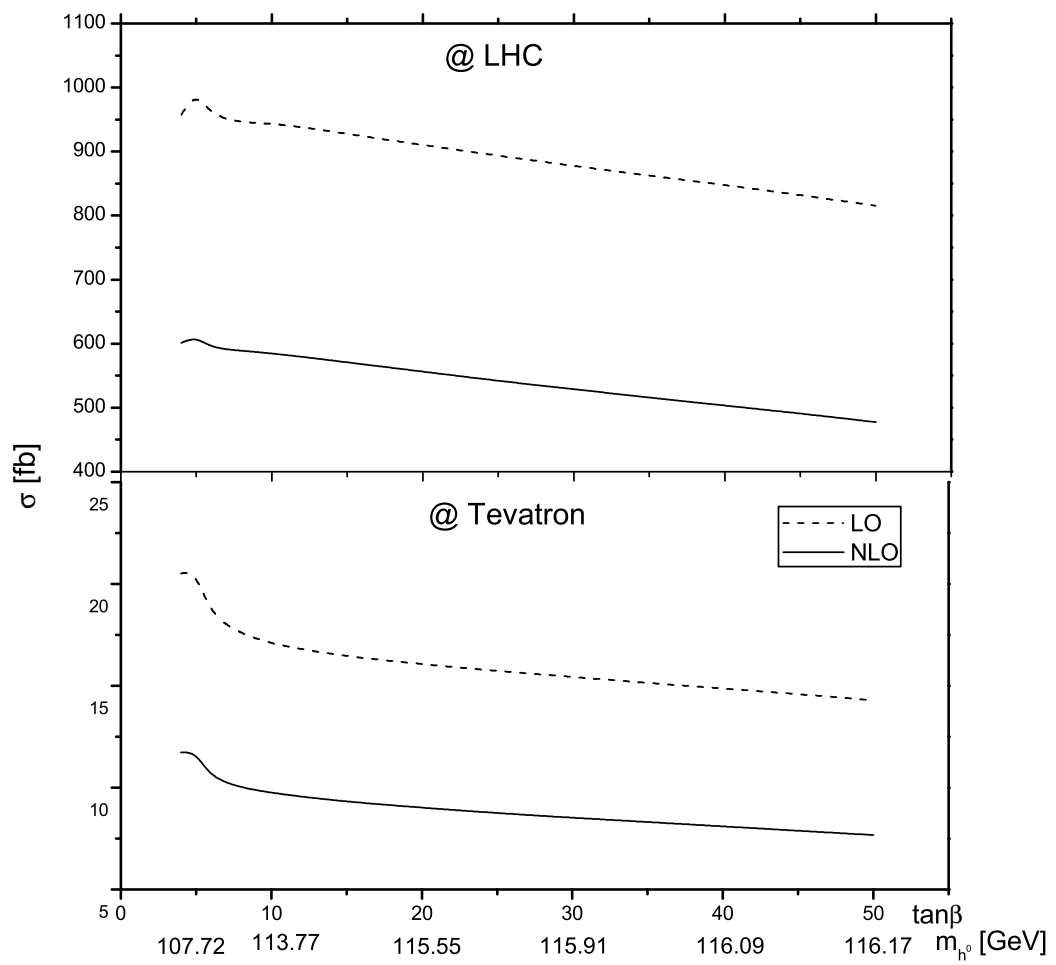


Fig.9

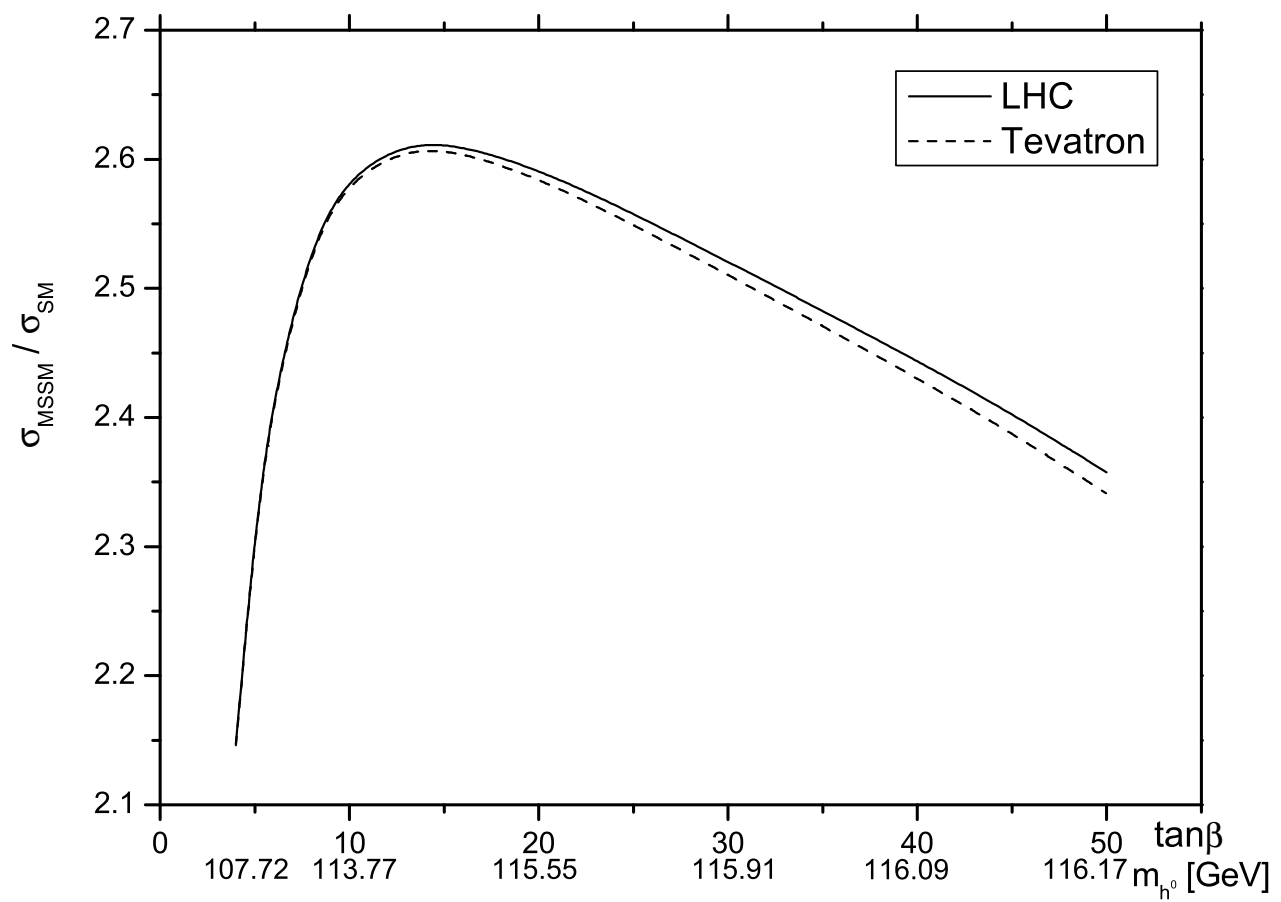


Fig.10

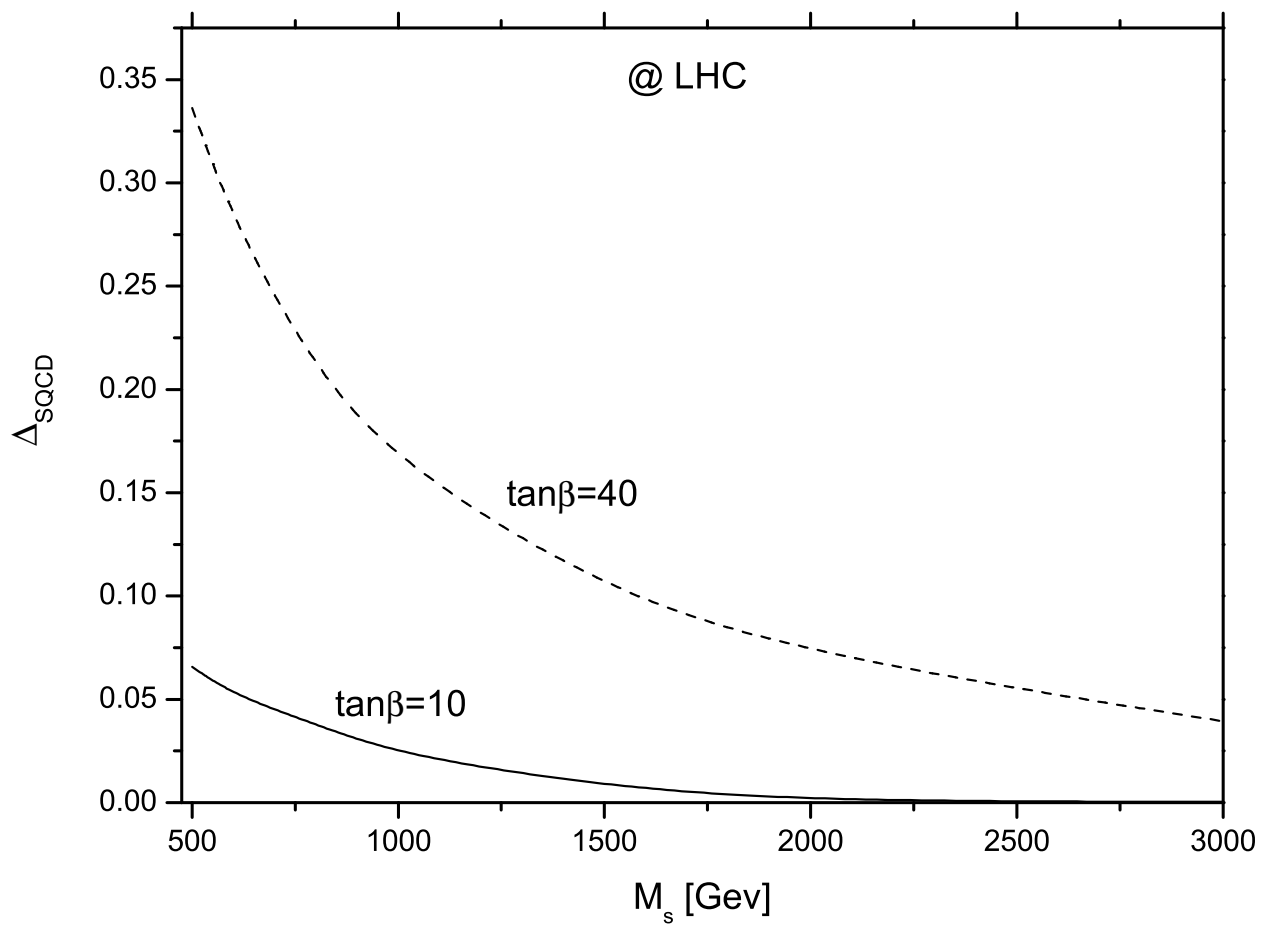


Fig.11

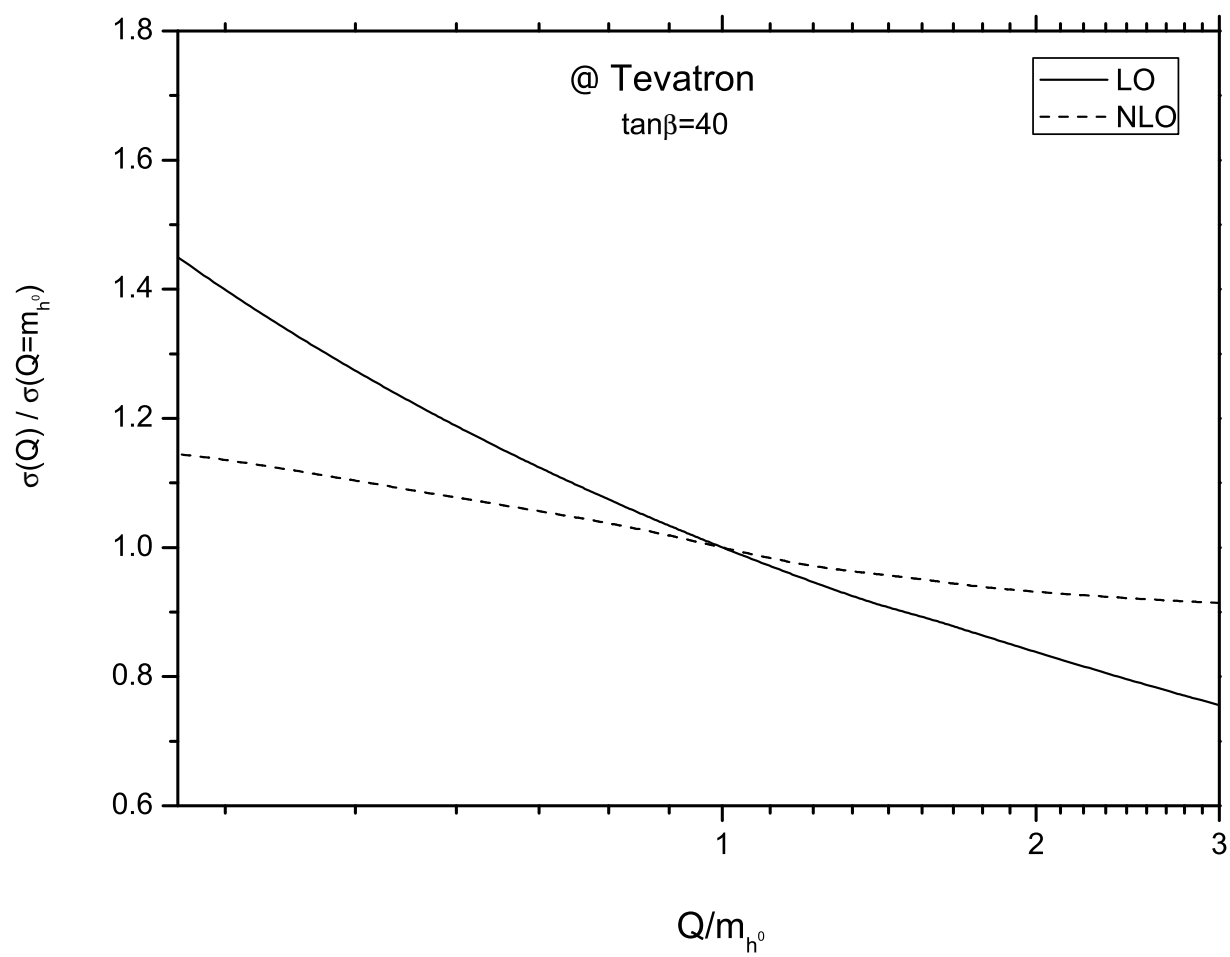


Fig.12